

# Examining the early stages of the thermal oxidative degradation in epoxy-amine resins

Suzanne Morsch<sup>a,\*</sup>, Yanwen Liu<sup>a</sup>, S.B. Lyon<sup>a</sup>, S.K. Gibson<sup>a</sup>, Benjamin Gabriele<sup>c</sup>, Mikhail Malanin<sup>d</sup>, Klaus-Jochen Eichhorn<sup>d</sup>

<sup>a</sup> Corrosion and Protection Centre, Department of Materials, The University of Manchester, The Mill, Sackville St, Manchester, M13 9PL, UK

<sup>b</sup> AkzoNobel, Stoneygate Lane, Felling, Gateshead, NE10 0JY, Tyne and Wear, UK

<sup>c</sup> Chemical Engineering and Analytical Science (CEAS), The University of Manchester, The Mill, Sackville St, Manchester, M13 9PL, UK

<sup>d</sup> Abteilung Analytik, Institut Makromolekulare Chemie, Leibniz-Institut für Polymerforschung Dresden e.V., Hohe Str. 6, 01069, Dresden, Germany

## ARTICLE INFO

### Article history:

Received 26 January 2020

Received in revised form

12 March 2020

Accepted 12 March 2020

Available online 18 March 2020

### Keywords:

Epoxy-amine

Oxidation

Vibrational spectroscopy

## ABSTRACT

Epoxy-amine resins continue to find widespread use as the binders in protective and decorative organic coatings, as the matrix in composite materials, and as adhesives. In service, exposure to the environment ultimately results in oxidative deterioration of these materials, limiting the performance lifetime. Defining this auto-oxidation process is therefore a key challenge in developing more durable high-performance materials. In this study, we investigate oxidative degradation of a model resin based on diglycidyl ether of bisphenol-A (DGEBA) and an aliphatic amine hardener, triethylenetetraamine (TETA). Using infrared spectroscopy, we find that prior to the expected detection of formate groups (corresponding to the well-known radical oxidation mechanism of DGEBA), a band at  $1658\text{ cm}^{-1}$  forms, associated with amine cross-linker oxidation. Infrared microspectroscopy, in-situ heated ATR-infrared, Raman spectroscopy and AFM-IR techniques are thus employed to investigate the early stages of resin oxidation and demonstrate strong parallels between the initial stages of cured resin degradation and the auto-oxidation of TETA cross-linker molecules.

© 2020 The Authors. Published by Elsevier Ltd. This is an open access article under the CC BY license (<http://creativecommons.org/licenses/by/4.0/>).

## 1. Introduction

Epoxy-amine resins continue to find widespread use as the binders in protective and decorative organic coatings, as the matrix in high performance composite materials, and as adhesives. During service, exposure to the environment ultimately results in deterioration of the polymer network (particularly in the case of exterior coatings and construction materials), and this is known to limit performance lifetime [1].

For thermoset polymers, it is well-known that aging can be subcategorized into physical processes affecting the network topology, and changes to the chemical structure. The former occurs via slow molecular relaxation in the glassy state (below the  $T_g$ ), which results in a reversible reduction in the free volume, and enthalpy recovery [2]. This ubiquitous type of aging is dependent on the thermal history of the sample, and is associated with some problematic phenomena including embrittlement and densification. The second type of aging, involving chemical damage, is more

closely associated with network deterioration and failure, but less understood. Irreversible chemical changes are known to occur as a result of polymer oxidation, and are often accompanied by lowering of the  $T_g$  [3], a loss of adhesion [4,5], yellowing [6] and cracking [7]. Despite this, the auto-oxidation mechanisms of common resins have not been defined, even in the case of the simplest and most widely studied class of thermosets, solventless cold-cure epoxy amine resins. In this study, we examine the early stages of oxidative degradation of a model epoxy-amine resin based on diglycidyl ether of bisphenol-A (DGEBA) and an aliphatic amine hardener, triethylenetetraamine (TETA), since this system falls within the most widely studied group of epoxies and amine hardeners (i.e., those based on ethylene diamine (EDA) building block; including EDA, diethylenetriamine (DETA) and TETA).

In recent decades, numerous studies have used infrared spectroscopy to identify the oxidation products of epoxy resins. For epoxies based on the diglycidyl ether of bis-phenol-A (DGEBA) unit, several characteristic spectral changes have consistently been identified after photo- or thermal aging, both in the absence of cross-linkers (phenoxy resins), and in networks formed using anhydride or amine hardeners. As a result, a broad consensus has

\* Corresponding author.

E-mail address: [Suzanne.morsch@manchester.ac.uk](mailto:Suzanne.morsch@manchester.ac.uk) (S. Morsch).

been reached on the dominant auto-oxidation mechanism involving the DGEBA repeat unit [8–14]; Initiation involves hydrogen abstraction from the  $\alpha$ -CH<sub>2</sub> adjacent to the phenyl ether group, followed reaction with molecular oxygen for the formation of peroxy macroradicals. Conversion to alkoxy radicals, and subsequent  $\beta$ -scission reactions then yield formate end groups, which constitute the main oxidation products from this part of the resin [12]. This process is consistently characterised by attenuated absorption at 1039 cm<sup>-1</sup> (phenyl ether region) and the growth of a band at 1739 cm<sup>-1</sup> (corresponding to formate groups) [11–14]. A second, more minor pathway to formate generation has also been identified via CH<sub>2</sub> hydrogen abstraction from isopropylidene sites [12].

Despite these advances in understanding, attempts to fully characterise oxidation in cross-linked epoxy networks remain hampered by the broad, ill-defined infrared bands emergent after oxidation, and the accepted contribution of complex alkoxy radical chemistry, which yields an abundance of possible mechanisms. For example, the appearance of a band around 1660 cm<sup>-1</sup>–1670 cm<sup>-1</sup> is specifically characteristic of an amine-related aging mechanism, since it is known to be dependent on amine content [8], and has not been observed for photo-oxidised phenoxy resins [9,12] or epoxy-anhydride resins [11,14,15]. The band appears for aged epoxies cross-linked with aliphatic or aromatic amine hardeners [16–18] after thermal aging [19,20], hygrothermal cycling [5,21], UV exposure [22,23] and outdoor weathering [7,24,25]. However, in cases where a functional group has been assigned to this band, there is no consensus; it has variously been attributed to alkenes [20], diphenyl ketones [26], amide groups [17,27,28], imine/oxime formation [20], quinones [7], or simply carbonyl functionalities [5,21].

In this study, we examine the origin of oxidation products associated with the amine cross-linker. The emergence of infrared bands is initially tracked using ATR-FTIR, and we find that during oxidation under mild conditions, the growth of absorption at 1658 cm<sup>-1</sup>, associated with amine cross-linker oxidation, precedes that at 1738 cm<sup>-1</sup>, which is characteristic of DGEBA oxidation. The early stages of resin oxidation are thus examined in detail, in order to isolate the mechanism of amine oxidation. Due to the small spectral changes visible after short oxidation times, this is achieved using a range of advanced vibrational spectroscopy tools; ex-situ ATR-infrared microspectroscopy, in-situ temperature-controlled ATR-infrared spectroscopy, Raman spectroscopy and nanoscale cross-sectional AFM-IR. Oxidation of the molecular amine hardener is also fully characterised, and we find significant parallels between the aliphatic amine oxidation products and those found in the resins during the early stages of thermal aging.

## 2. Experimental

### 2.1. Sample preparation

The epoxy-amine resins used consisted of stoichiometric (1:3 M ratio TETA:DGEBA) mixtures of diglycidyl ether of bisphenol-A (DGEBA) epoxy and triethylenetetraamine (TETA) hardener (Araldite 3138 and Aradur 3140 respectively, Huntsman), Scheme 1. The components were thoroughly mixed for 90 s at 1500 rpm (Speed-Mixer DAC150). The mixture was poured into polypropylene moulds and cured at room temperature for 48 h before removal from the moulds. Finally post-cure heating was performed at 120 °C for 1 h. In order to remove any 'skin' layer on formed at the polymer-air interface, all specimens were abraded on both sides with 600 and 1200 grit silicon carbide paper, and rinsed in deionised water before storage in a desiccator.

Resin aging was performed by exposure to four different environmental conditions: ambient laboratory conditions (30–40% RH,

22 °C), immersion in deionised water (pH 6) at room temperature (22 °C), exposure to 70 °C at 80% RH in a humidity cabinet (Memmert Climate Chamber), and under dry conditions at 70 °C (over silica desiccant, measured humidity of 14% RH, in a drying oven).

### 2.2. Fourier Transform Infrared (FTIR) spectroscopy

ATR (attenuated total reflection)-FTIR (Fourier Transform Infrared) spectroscopy of epoxy amine samples after aging at 70 °C under 14% RH for periods of up to 118 days were obtained using a FTIR-spectrometer (Nicolet 5700 spectrometer, Thermo Electron Corp.) equipped with room-temperature DTGS (deuterated triglycine sulfate) detector operating at 4 cm<sup>-1</sup> resolution across the 4000–500 cm<sup>-1</sup> range. 64 co-averages were added to every spectrum.

Detailed ATR-FTIR spectra of epoxy amine resins after the early stage of aging (28 days) were measured using an FTIR-microscope (Hyperion 2000, Bruker) equipped with both 20x-ATR-Objective (numerical aperture 0.6, Ge-ATR-crystal, measurement spot is about 25  $\mu$ m, penetration depth < 500 nm at 1000 cm<sup>-1</sup>) and liquid nitrogen cooled mercury-cadmium-telluride (MCT) detector (InfraRed Associates Inc.). The FTIR-microscope was coupled with FTIR-spectrometer Vertex 70 (Bruker). Spectral resolution and spectral range were 4 cm<sup>-1</sup> and 4000–600 cm<sup>-1</sup> respectively. 100 scans were co-added to every spectrum. Each sample had 10 measurement spots and if necessary an average spectrum of these 10 measurements has been calculated.

In-situ temperature dependent FTIR-spectroscopy of the TETA hardener was performed on a Vertex 80v (Bruker) using a heated Golden Gate Diamond ATR unit (SPECAC), equipped with a liquid nitrogen cooled mercury-cadmium-telluride (MCT) detector. Spectra were gathered over 4000–600 cm<sup>-1</sup> range with a spectral resolution of 4 cm<sup>-1</sup>, 100 scans were co-added to each spectrum. Measurements were carried out in the temperature range from room temperature (RT) to 120 °C (at RT, 40, 80, 120 °C) at 40–45% RH. Every temperature point was stabilised for 15 min, and at 120 °C the sample was held for 60 min, whilst acquiring ATR-spectra of the sample every 5 min. To exclude temperature influence on band intensity, the spectra were referenced to blank ATR-crystal heated up to the same temperature points.

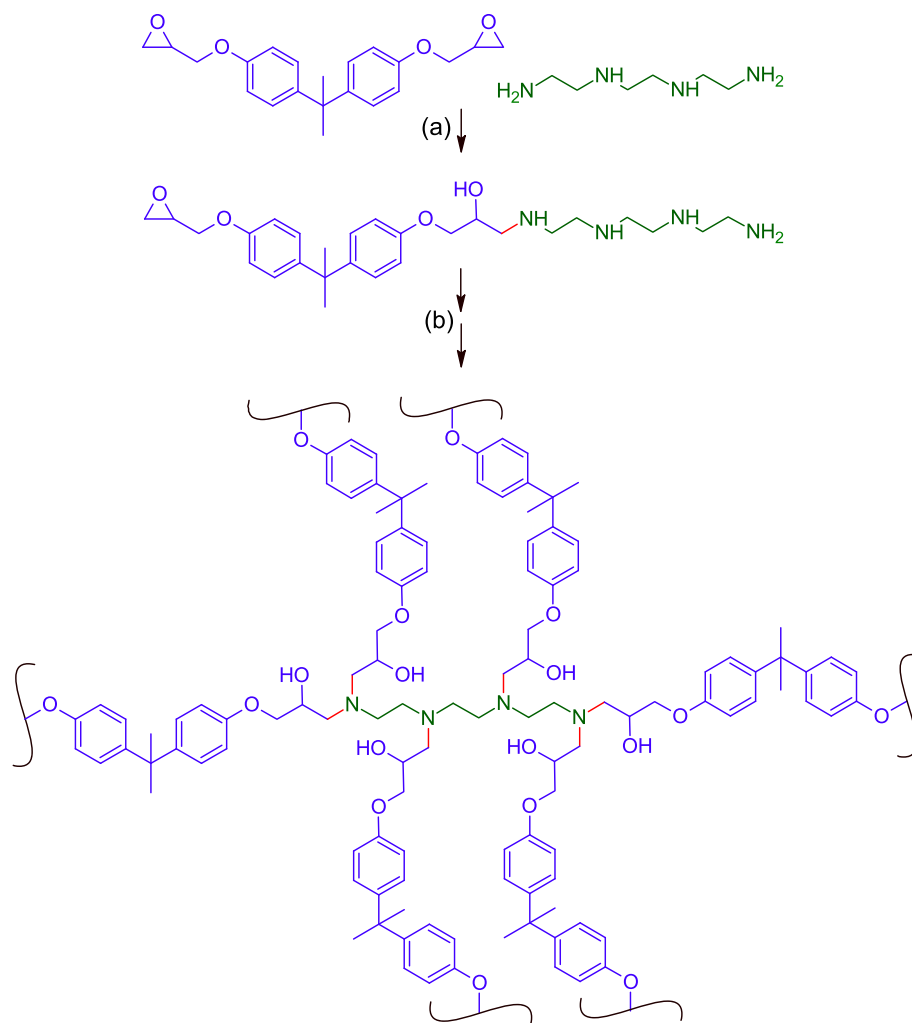
In both cases, spectral processing involved atmospheric and baseline correction as well as a normalization and spectral subtraction. ATR-spectra of epoxy-amine resins have been normalised relative to the band of the aromatic ring stretching vibration at 1504 cm<sup>-1</sup> [29,30]. Temperature controlled ATR-spectra of TETA were normalised using the scissor vibration band of methylene group at 1455 cm<sup>-1</sup>. Characteristic infrared bands are assigned using references 29 and 30.

### 2.3. Raman spectroscopy

Raman spectroscopy was performed at room temperature using a LabRam 300 confocal Raman microscope (Horiba) equipped with a HeNe laser (incidence radiation wavelength of 632.82 nm). Calibration was performed with a Silicon (Si) calibration sample prior to the measurements, which were carried out using a 100 x objective, 600 grating, a 2 s acquisition times over the 600 cm<sup>-1</sup> – 900 cm<sup>-1</sup> range, and 2 accumulations per spectrum. The residence time distribution (RTD) was 1 s.

### 2.4. AFM-IR

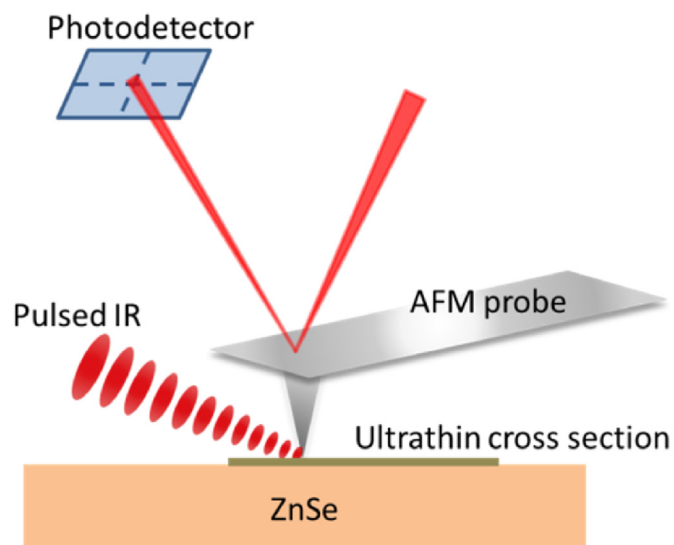
Nanoscale infrared analysis (AFM-IR) was performed on an Anasys NanoIR3s system (Bruker) operating with top-down illumination. To assess the internal nanostructure, polymer sections of



**Scheme 1.** The structure of resin constituents (diglycidyl ether of bisphenol-A and triethylenetetraamine) and the reaction (a) between the epoxy and primary amine groups to form a secondary amine junction and (b) the complete reaction of all amine moieties to form a cross-linked network.

200 nm nominal thickness were prepared using an ultramicrotome (Leica EM UC6) with a diamond knife. Sections were collected on transmission electron microscopy (TEM) grids, then floated onto a droplet of deionised water placed on a ZnSe substrate. Upon evaporation of the droplet, TEM grids were removed, specimen sections remained on the ZnSe surface, and these were dried for >16 h in a desiccator prior to examination.

During AFM-IR analysis, the microtomed sections were illuminated by a pulsed tunable QCL laser, [Scheme 2](#). Sub-diffraction limit resolution is achieved by monitoring the deflection of an AFM probe in contact with the surface. This results from rapid transient thermal expansion of the material in contact with the probe tip in response to infrared absorbance [31]. The recorded AFM-IR signal is the amplitude of induced AFM probe oscillation, obtained after fast Fourier transform. Stepping the incident radiation through the infrared fingerprint region and recording the amplitude in this way has previously been shown to generate spectra closely matched to those measured using conventional macroscopic FTIR [32]. For imaging, simultaneous contact-mode topographical measurement and infrared mapping can be performed by holding the incident laser at a given wavelength during scanning [33–36]. In the present study, AFM-IR images were collected in resonance enhanced contact mode at a scan rate of 0.5 Hz using a gold-coated silicon nitride probe (0.07–0.4 N/m spring constant,  $13 \pm 4$  kHz resonant



**Scheme 2.** The AFM-IR experimental set-up with top-down illumination.

frequency, Bruker). Spectra were collected using 261 points over a range of  $1280\text{ cm}^{-1} - 1800\text{ cm}^{-1}$  at a sample rate of 12.5 MHz. In both cases, the pulse rate was matched to the resonant frequency of the cantilever, and was maintained at a repetition rate of approximately 180 KHz via a PLL feedback loop. For mapping, the amplitude of infrared induced oscillation was recorded at a given wavelength using 600 points per 100 scan lines. Sets of spectra and images were collected in three different regions to ensure reproducibility.

### 3. Results and discussion

#### 3.1. Ex-situ ATR-FTIR

Cured DGEBA-TETA resins were examined periodically using ATR-FTIR with a single bounce diamond internal reflection element (IRE) over the course of 118 days (>2800 h) exposure to  $70\text{ }^{\circ}\text{C}$  under dry conditions (14% RH), Fig. 1. These mild conditions were selected to be relevant for external corrosion protective coatings or construction materials. Previous reports have demonstrated that epoxy resins aged for thousands of hours under mild accelerated conditions (UV illumination,  $60\text{ }^{\circ}\text{C}$ ) produce chemical changes comparable to those induced by prolonged storage under ambient conditions (1 year) [37]. Moreover, it has also been reported that the use of high temperatures (> $110\text{ }^{\circ}\text{C}$ ) to further accelerate oxidation can change the oxidation chemistry via the preferential activation of mechanisms such as Copeland elimination and dehydration reactions [20,38].

Examination of the epoxy-amine infrared fingerprint regions reveals the expected emergence of bands at  $1658\text{ cm}^{-1}$  and  $1738\text{ cm}^{-1}$ , corresponding to oxidation products. Integration and normalization of these bands however indicates that the two products are not generated in a concerted fashion. This is in keeping with a recent study by Meiser et al. examining the low angled microtome cross-sections of similarly thermally aged DGEBA-DETA

resins [20]. In that study, detailed profile analysis revealed that the absorption bands at  $1660\text{ cm}^{-1}$  and  $1725\text{ cm}^{-1}$  also did not develop in a synchronous manner after 300 days aging at  $60\text{ }^{\circ}\text{C}$ . Furthermore, in the present study an induction period of 38 days is observed before formate species are weakly detected, a comparable timescale to the 400 h (17 days) induction period reported elsewhere for this band during thermal oxidation of DGEBA-DETA resins aged at  $100\text{ }^{\circ}\text{C}$  [17]. In contrast, no induction period is observed for the appearance of the  $1658\text{ cm}^{-1}$  band, indicative of a distinct initiation mechanism. The  $1738\text{ cm}^{-1}$  band can be assigned to formate end groups produced by the well-known hydrogen-abstraction radical initiation mechanism of DGEBA auto-oxidation [12]. This mechanism is accompanied by the consumption of the phenyl ether and isopropylidene groups (signified by a loss of absorption at  $1040\text{ cm}^{-1}$  and  $1183\text{ cm}^{-1}$ ). The absence of any detectable consumption of these bands in the present case therefore provides supporting evidence of a separate initiation mechanism generating the absorption band at  $1658\text{ cm}^{-1}$ .

In order to selectively examine the mechanism of early stage oxidation (in the absence of DGEBA oxidation pathway) cured resins were therefore exposed to three different mild oxidative environments for just 28 days (i.e., prior to the detection of formate groups):  $70\text{ }^{\circ}\text{C}$  under humid (80% RH) or dry (14% RH) conditions, and immersion in deionised water at  $22\text{ }^{\circ}\text{C}$ . Control samples were stored under ambient laboratory conditions ( $22\text{ }^{\circ}\text{C}$  and 30–40% RH). Since spectral changes are minor at such early stages, the aged resins were examined using a more sensitive approach: 10 spectra were acquired using an ATR-FTIR microscope equipped with automated sampling and a germanium internal reflection element (sampling depth < 500 nm). As a result, the epoxy-amine spectra were found to be highly reproducible, allowing minor changes in absorption to be detected, Fig. 2. As expected, after aging for 28 days, visible spectral changes were limited to the emergence of a broad absorbance band around  $1658\text{ cm}^{-1}$ . Integration revealed that the growth of this band was accelerated by heat, and by the

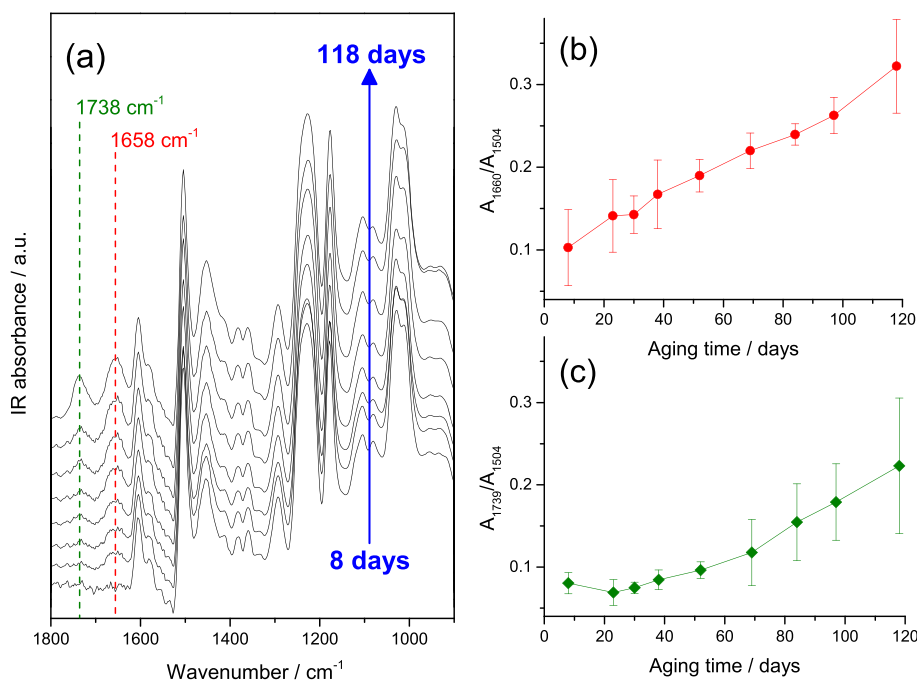


**Fig. 1.** (a) ATR-FTIR spectra of stoichiometric DGEBA-TETA epoxy-amine resins after 48 h ambient cure and 1 h  $120\text{ }^{\circ}\text{C}$  post cure heating followed by aging at  $70\text{ }^{\circ}\text{C}$  under dry (14% RH) conditions for 8, 23, 38, 52, 69, 84, 97 and 188 days; and the integrated absorption band areas at (b)  $1658\text{ cm}^{-1}$  and (c)  $1738\text{ cm}^{-1}$  as a function of aging time. Band areas are the mean of 5 individual measurements, normalised to the area of the aromatic  $1504\text{ cm}^{-1}$  band in each case. Error bars correspond to one standard deviation.

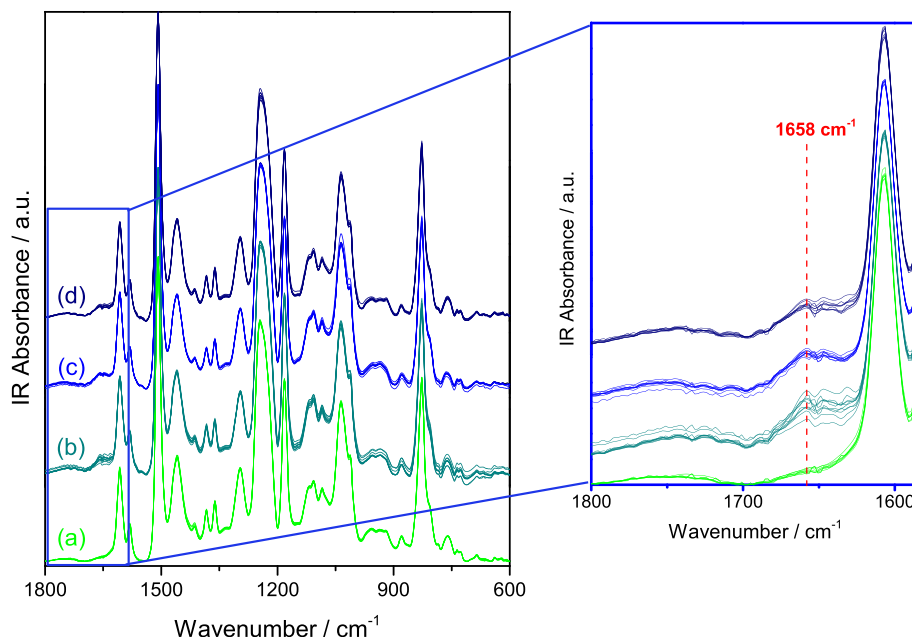


**Fig. 2.** ATR-FTIR spectra of stoichiometric DGEBA-TETA epoxy-amine resins after 48 h ambient cure and 1 h 120 °C post cure heating followed by (a) 4 weeks of storage at 22 °C and ~40% RH (ambient conditions); (b) aging for 4 weeks at 70 °C under dry (14% RH) conditions; (c) aging for 4 weeks at 70 °C under humid (80% RH) conditions and (d) 4 weeks immersion in deionised water at 22 °C. Spectra have been normalised relative to the aromatic ring stretching vibration band at 1504 cm<sup>-1</sup>.

presence of water (i.e., in a humid environment, when compared to dry conditions at 70 °C, and during immersion at 22 °C, when compared to the control samples stored under ambient humidity at 22 °C), Table 1.

More importantly, due to the reproducibility of the spectra, more detailed analysis of chemical changes was also possible by the examination of difference spectra. These were generated by subtracting the averaged spectrum obtained for the control sample from those gathered after accelerated aging of the resins, Fig. 3. In addition to the absorbance band seen in the original spectra at 1658 cm<sup>-1</sup>, the emergence of a second infrared band centred around 1592 cm<sup>-1</sup> was identified. Negative bands were also evident across the rest of the fingerprint region, generally appearing in comparable proportions to (positive) absorbance bands in the original spectra. As such, these can mostly be ascribed to subtraction artefacts, or to network swelling. It is however notable that disproportionately intense negative bands associated with the consumption of CH<sub>2</sub> groups appeared after aging under high temperature conditions (found at 1455 cm<sup>-1</sup> and 1301 cm<sup>-1</sup>, corresponding to disappearance of the CH<sub>2</sub> scissor vibration and CH<sub>2</sub> deformation respectively) [29,30]. Since the aforementioned integration of the 1658 cm<sup>-1</sup> band indicated that oxidation was more advanced after aging at 70 °C, this indicates that CH<sub>2</sub> consumption is associated with the oxidation process. This supports the idea that the incorporated TETA molecule is attacked, since this is where the majority of CH<sub>2</sub> groups reside within the resins, Scheme 1.

**Table 1**

Area of the infrared absorbance band around 1660 cm<sup>-1</sup> for stoichiometric DGEBA-TETA epoxy-amine resins after 48 h ambient cure and 1 h 120 °C post cure heating followed by 4 weeks aging under various conditions. Measurements correspond to the mean value obtained for 10 spectra normalised to the 1504 cm<sup>-1</sup> band (see Fig. 1), errors correspond to one standard deviation.

Aging Conditions	Area of 1660 cm <sup>-1</sup> IR absorbance band
22 °C, ~40% RH	N/A
22 °C, water	0.81 ± 0.39
70 °C, 14% RH	0.80 ± 0.13
70 °C, 80% RH	0.95 ± 0.09

### 3.2. In-situ ATR-FTIR

Since the incorporated TETA molecule was identified as a likely site of attack, auto-oxidation of the TETA molecule was examined in detail using in-situ temperature-controlled ATR-FTIR, Fig. 4. Unlike the fully cross-linked resins, the simplicity of this molecule allowed the identification of all infrared bands, predominately using references 29 and 30. During this experiment, spectra were acquired every 5 min as the temperature was gradually increased to induce an oxidation reaction.

Fig. 4a shows the effect of warming the amine from refrigeration temperature (4 °C) to 40 °C and then to 80 °C. It can be seen that the amine rapidly adsorbs water at 40 °C, as expected due to its hygroscopic nature. Water uptake was identified by the increased intensity and broadening of the band at 3279 cm<sup>-1</sup> (corresponding to the water OH-group stretching vibration), as well as the appearance of a shoulder at 1657 cm<sup>-1</sup> (OH deformation vibration) [29,30]. Additionally, water uptake induced some changes in the spectrum below 1000 cm<sup>-1</sup>. This is a result of overlap between the hydrogen-bonded bending and stretching vibrations of liquid water and the C–N–H wagging of primary (at 899 cm<sup>-1</sup> and 812 cm<sup>-1</sup>) and secondary (at 767 cm<sup>-1</sup>) amines [39]. Confirmation that these changes correspond to water sorption was provided upon further heating to 80 °C, since this initiates dehydration, and hence results in all of the aforementioned bands becoming simultaneously attenuated.

At the same time as the growth of water bands, the growth of a band appearing at 1301 cm<sup>-1</sup> occurs. This corresponds to a stretching vibration of N–C in carbamate -N-COO<sup>-</sup> ion, which is known to be formed by reaction of water and CO<sub>2</sub> with primary or secondary amines [40,41]. The formation of this band is, however, reversible upon further heating after water loss (see the spectrum of TETA after 0 min at 120 °C, Fig. 4b). Moreover, at no point during the in-situ experiment were the characteristic carbamate bands observed (asymmetric and symmetric COO<sup>-</sup> vibrations, typically found in the regions of 1600 cm<sup>-1</sup> - 1500 cm<sup>-1</sup> and 1450 cm<sup>-1</sup> - 1350 cm<sup>-1</sup>) [40,41], nor was any characteristic blush observed on

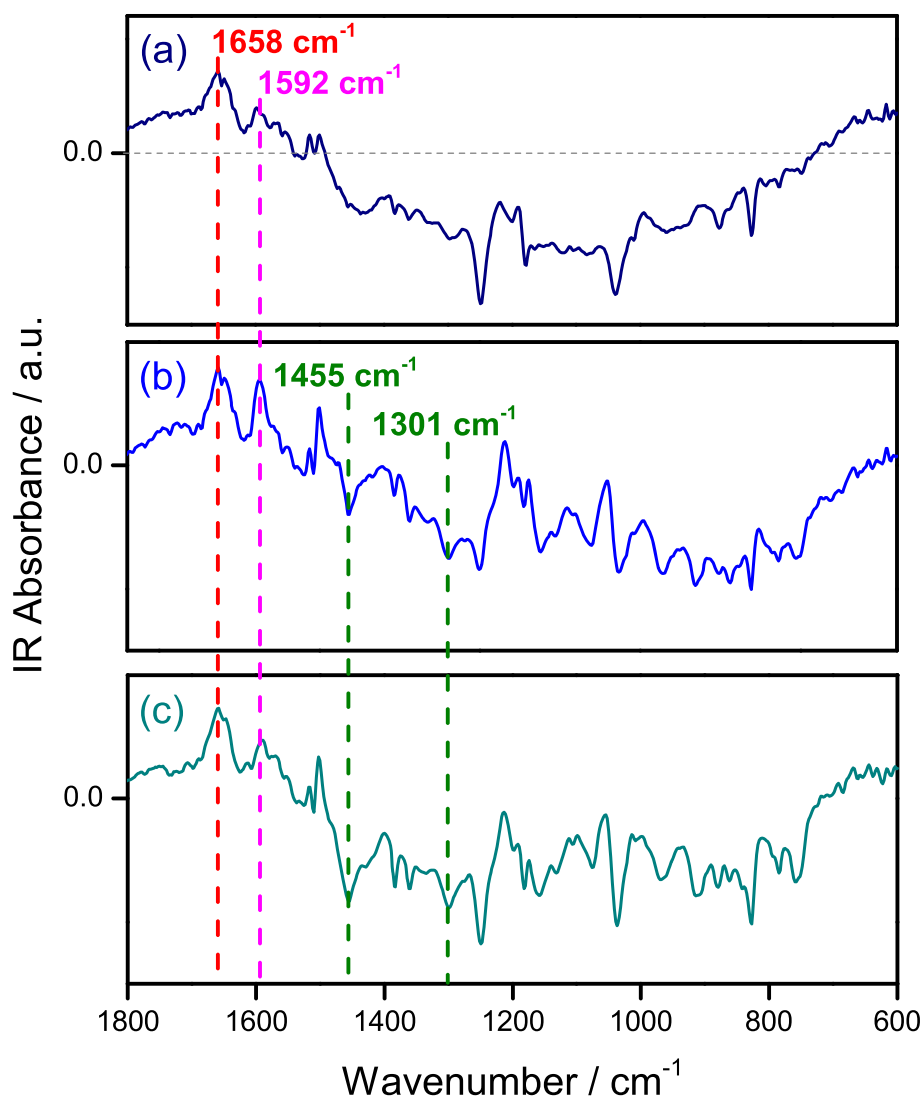


**Fig. 3.** Infrared difference spectra obtained by subtracting the average ATR-FTIR spectrum of epoxy amine specimens stored under laboratory conditions for 4 weeks (22 °C, 40% RH) from the average spectra obtained for: (a) epoxy-amine resins aged at 22 °C for 4 weeks by immersion in deionised water; (b) epoxy-amine resins subjected to 70 °C and 14% RH for four weeks and (c) epoxy-amine resins subjected to 70 °C and 80% RH for four weeks.

the surface of cold cured resin specimens, indicating that carbamate is not a significant side reaction consuming the molecular amine during the ambient cure of resins.

After dehydration and carbamate decomposition, heating to 120 °C produced a spectrum comparable to that of the fresh TETA sample, Fig. 4b. When the amine was held at 120 °C however, the spectrum was observed to progressively change over the course of 60 min monitoring, indicating that an oxidation reaction occurred. The most remarkable changes were found in the region of amine group vibrations; after 20 min a new band was detected at 1668  $\text{cm}^{-1}$  (corresponding to stretching vibration of C=N oscillation pair in imine), and further heating led to the unambiguous growth of this band as well as one at 1596  $\text{cm}^{-1}$  (C=N stretching vibration in azadiene and/or bending vibration of N-H in C=N-H group) [29,30].

The growth of bands at 1668  $\text{cm}^{-1}$  and 1596  $\text{cm}^{-1}$  coincides with the development of a new band at 3109  $\text{cm}^{-1}$  (stretching vibration of associated C=N-H groups in the imine), alongside a broadening and red shift of the amine N-H stretching vibration bands, from 3290  $\text{cm}^{-1}$  to 3217  $\text{cm}^{-1}$  [29,30]. This confirms the presence of new and strongly hydrogen bonded functionalities,

since the disruption of amine hydrogen bonding expected at high temperatures would result in a blue band shift [42]. Furthermore, there are significant attenuations of numerous bands in the 1200  $\text{cm}^{-1}$  - 600  $\text{cm}^{-1}$  region, including the symmetric stretching vibrations of C-N-C in secondary amines (at 1124  $\text{cm}^{-1}$ ), and the C-N-H wagging vibrations of both primary (at 899  $\text{cm}^{-1}$  and 812  $\text{cm}^{-1}$ ) and secondary (at 767  $\text{cm}^{-1}$ ) amines [29,30]. It is, however, notable that the band at 812  $\text{cm}^{-1}$  remains in the spectrum even after 60 min exposure to 120 °C, indicating that primary amines are consumed less dramatically than secondary amines. Taken in combination with band changes in the N-H stretching range, one can deduce that a structural transformation of the amines in TETA to imine/azadiene groups takes place, whilst some amount of primary amine is preserved. This is also accompanied by a change of band ratio 2929  $\text{cm}^{-1}$ /2807  $\text{cm}^{-1}$  (asymmetric and symmetric stretching vibration bands of CH<sub>2</sub> group respectively), and a reinforcement of the band of CH<sub>2</sub> twisting vibration in imines at 1294  $\text{cm}^{-1}$  [29,30].

Finally, the appearance of weak bands at both 2208  $\text{cm}^{-1}$  (stretching vibration of C≡N group in unsaturated nitriles) and 2142  $\text{cm}^{-1}$  (stretching vibration of isonitrile group) can also be

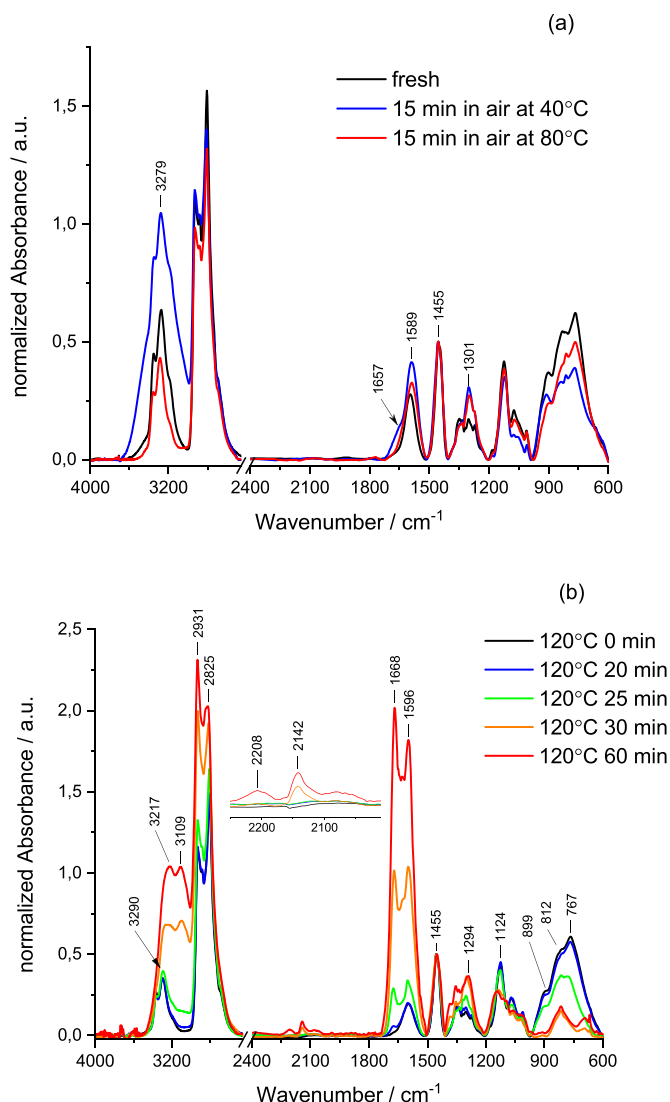


**Fig. 4.** In-situ ATR-FTIR spectra of triethylenetetramine cross-linker (a) at 4 °C (after removal from refrigerator) and after warming to 40 °C and holding for 15 min, then 80 °C and holding for 15 min, and (b) after further warming to 120 °C and holding for 15 min, 20 min, 25 min, 30 min, 55 min and 60 min.

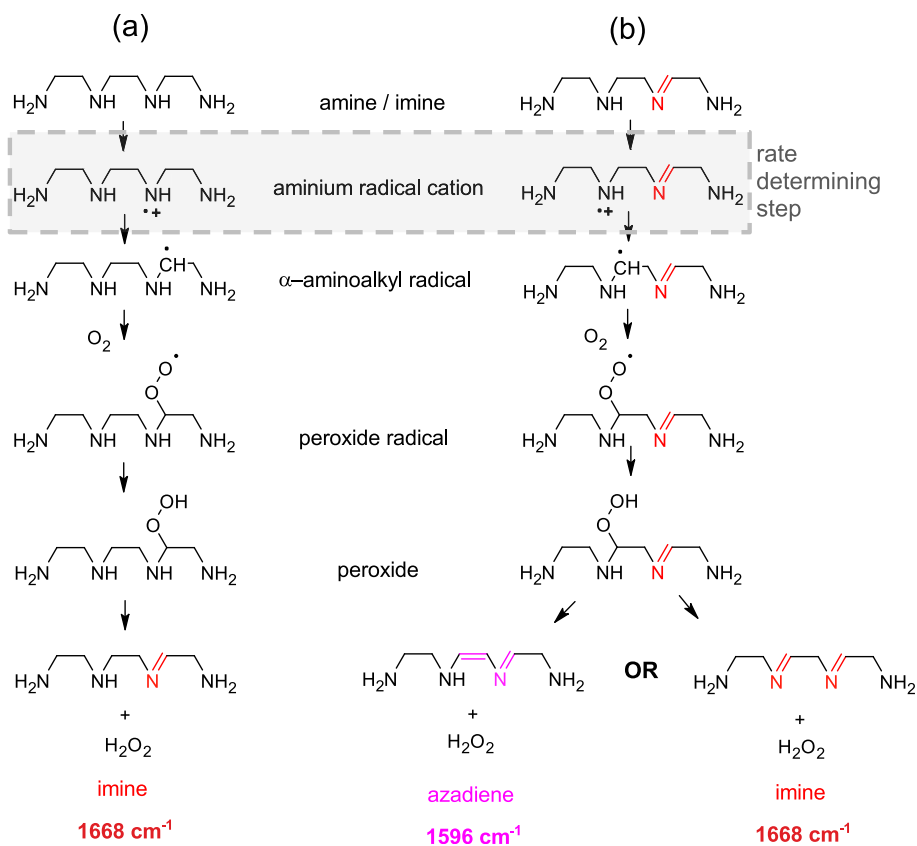
discerned after 60 min heating at 120 °C. These groups may form as a consequence of a side reaction involving the oxidation of primary amines [43,44]. This reaction is however considered irrelevant to the oxidation of resins, since neither primary nor secondary amine groups are, of course, present in the fully reacted epoxy amine resin, having been converted into tertiary amine groups. This is also the case for carbamation reactions.

Nonetheless, the preferential attack of secondary amines does provide an important clue about the auto-oxidation mechanism of TETA incorporated into resins. This is because preferential reaction of secondary amines is characteristic of a radical oxidation mechanism. Facile oxidation of amines via electron abstraction has previously been reported to occur in the presence of one-electron oxidants [45–47], and more importantly, the same mechanism is considered to underpin the auto-oxidation of amines [48,49]. In both cases, the reactivity of amines follows the order of tertiary > secondary > primary since the first rate-limiting step results in the formation of a radical aminium cation, and this intermediate is stabilised by inductive effects.

Furthermore, the literature concerning one-electron oxidation of amines also supports the proposed formation of imines [45–49], and this is in keeping with the known chemistry of aminium radical cations, which has been studied in recent years due its potential utility in green chemical syntheses [50]. The spontaneous thermal oxidation of molecular amines used as carbon-dioxide scrubbers has also been shown to proceed via comparable mechanisms involving the formation of transient imine species [51]. Based on this body of literature and the infrared band assignments above, a dominant oxidation mechanism of TETA is proposed in Scheme 3. Note that this is proposed to be the preferential, rather than the sole, mechanism of oxidation. In-situ FTIR also indicated that numerous less prevalent oxidation reactions occurred, including the transformation of primary amine moieties to imine and nitrile groups (not shown).

According to the proposed mechanism, electron abstraction from a secondary amine initially results in the formation of an aminium radical cation. The identity of the initial one electron oxidant is not clear, but molecular oxygen, or radicals derived from the UV-chromophoric aromatic groups in DGEBA, known to initiate photo-aging of closely related phenoxy resins, could be responsible (since in the present case, aging was not performed in the dark) [8,9]. Once formed however, it is known that aminium radical cations rapidly rearrange to form the  $\alpha$ -aminoalkyl radicals, Scheme 3a. These can then be converted to radical iminium ions directly via further one-electron oxidation [50], or, since the aminoalkyl radical is vulnerable to attack by molecular oxygen, form peroxide species [51]. Unsaturated imine groups are then readily generated by the elimination of hydrogen peroxide. Similar attack of the second secondary amine moiety in TETA can then be envisaged to result in either the formation of another imine, or the formation of azadiene groups, Scheme 3b. The C=C bond produced in the azadiene product would be stabilised by conjugation with the adjacent imine, and is therefore anticipated to be a preferred product. Moreover, this second reaction route explains the concerted growth of bands at 1667 cm<sup>-1</sup> and 1592 cm<sup>-1</sup>, which can be attributed to in-phase and out-of-phase C=N–C=C stretches. A markedly similar set of bands have been reported at 1587 cm<sup>-1</sup>–1560 cm<sup>-1</sup> and 1664 cm<sup>-1</sup>–1657 cm<sup>-1</sup> in 2-azabutadiene [52], and comparisons can be made to butadienes, glyoximes and azines, where C=C–C=C and N=C–C=N in-phase and out-of-phase stretches also produce strong two infrared absorbance bands [29,53]. The similarity in the absorbance band intensities indicates that the bonds are coupled, with the di-imine being a minor product. Furthermore, whilst aliphatic imine groups are susceptible to hydrolysis under ambient conditions, it is noteworthy that after cooling overnight (>16 h at 22 °C), the spectrum of TETA oxidation products remained unchanged. This observation, alongside a notable yellowing during oxidation, supports the formation of azadiene products stabilised by conjugation.

Note that a very similar set of two bands appear in the difference spectra produced for aged resins (Fig. 3), alongside evidence of CH<sub>2</sub> group consumption. It is therefore proposed that the azadiene functional group is also produced during resin aging, via attack of the incorporated TETA molecules. In light of this, the oxidation of cured resins under mild conditions is unsurprising, since, despite steric restrictions, tertiary amines are even more vulnerable to one electron oxidation. This is because the tertiary aminium radical cations formed during the rate limiting initiation step are even more stable than the secondary species formed during the oxidation of TETA (due to superior inductive effects). Moreover, the formation of this transient radical ion will be stabilised by the presence of polar solvents, and the conformational transition to a planar configuration may be aided by water plasticization, providing an explanation for the acceleration of oxidative



**Scheme 3.** The auto-oxidation mechanism of TETA.

degradation in the presence of water. Whilst imine functional groups are generally considered unstable towards hydrolysis and further oxidation, conjugation in the form of azadiene groups may increase stability. It is notable that conjugated nitrogen compounds have repeatedly been proposed as an explanation for the enhanced discolouration of epoxy-amine resins aged by thermal means rather than UV oxidation, and that this has also been accompanied by an increased infrared absorbance around  $1660\text{--}1670\text{ cm}^{-1}$  relative to that at  $1739\text{ cm}^{-1}$  [8,13,17]. Nonetheless, it can be envisioned that ultimately, the products of imine hydrolysis may contribute to the observed broad oxidation bands around  $1658\text{ cm}^{-1}$  (primary amine N–H bend) and  $1738\text{ cm}^{-1}$  (aldehyde C=O, or carboxylic acid C=O stretch after further oxidation) in resins.

Importantly, this proposed mechanism differs substantially from the most commonly cited explanation for the oxidation band at  $1660\text{--}1670\text{ cm}^{-1}$ . Previously, investigators have proposed that since the concentration of species absorbing at  $1660\text{--}1670\text{ cm}^{-1}$  is known to depend on the concentration of  $\alpha$ -amino methylene content and the electron density on the nitrogen, this band forms as a consequence of hydrogen abstraction from the  $\alpha\text{-CH}_2$  group, followed by its oxidation to an amide [13,17,20,27]. Here, in order to ensure this was not the case, further evidence for the incorporation of imine and azadiene groups, rather than amides, into oxidised resins was sought using Raman spectroscopy.

### 3.3. Raman spectroscopy

Comparison of Raman spectra obtained for the control sample and for specimens exposed to accelerated aging conditions revealed very clear differences, Fig. 5. The most notable is the appearance of two strong peaks at  $1310\text{ cm}^{-1}$  and  $1360\text{ cm}^{-1}$ , which

dominate the Raman spectra of all three aged samples. All Raman bands were assigned using reference 29, and these corresponded to CH rocking vibrations on unsaturated C=C or C=N bonds.

In addition, strong bands associated with C=N and C=C stretches can be observed at  $1682\text{ cm}^{-1}$ ,  $1638\text{ cm}^{-1}$ ,  $1610\text{ cm}^{-1}$  and  $1568\text{ cm}^{-1}$ . In analogy with asymmetrically substituted butadienes, these can be considered to correspond to symmetric and asymmetric vibrations of the conjugated C=N and C=C groups [29]. The symmetric vibrations in particular would absorb more strongly in Raman spectroscopy than in infrared, and thus the distribution of bands is different. The presence of four bands can be attributed to the likely co-existence of several conformational isomers in the cured aged resin, and the fact that a greater number of possible amine oxidation sites will be present (four tertiary amines for every incorporated TETA molecule, Scheme 1). Finally, in keeping with the FTIR results and the proposed mechanism of attack, the  $\text{CH}_2$  scissors band at  $1460\text{ cm}^{-1}$  is completely consumed upon oxidation.

The appearance of strong C=N bands (comparable in intensity to the C=C band) are particularly important, since these effectively rule out the common assignment of amide formation as an alternative explanation for the infrared absorbance at  $1658\text{ cm}^{-1}$  (since polar amide groups generate weak Raman bands). A broad band in the carbonyl regions does however appear around  $1732\text{ cm}^{-1}$ . Since no increase in absorbance was seen in this region using two different FTIR approaches after 28 days aging, this is more likely to be a combination band than correspond to newly formed carbonyl functional groups.

### 3.4. AFM-IR

FTIR has previously been used to establish that the oxidative degradation of epoxy-amine resins initiates at the exposed

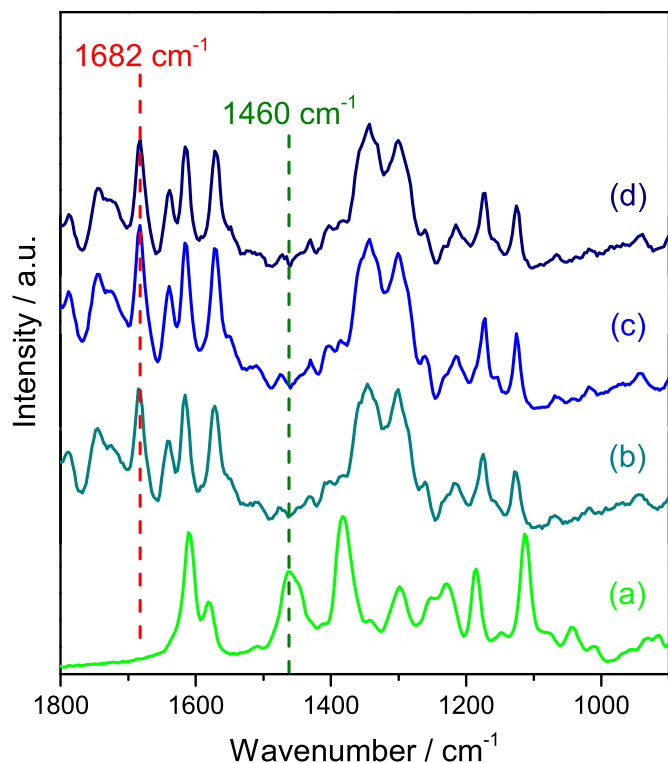


**Fig. 5.** Raman spectra of stoichiometric DGEBA-TETA epoxy-amine resins after 48 h ambient cure and 1 h 120 °C post cure heating followed by (a) 4 weeks of storage at 22 °C and ~40% RH (ambient conditions); (b) aging for 4 weeks at 70 °C under dry (14% RH) conditions; (c) aging for 4 weeks at 70 °C under humid (80% RH) conditions and (d) 4 weeks immersion in deionised water at 22 °C.

polymer-air interface and progresses gradually into the bulk. The location of degradation products at the surface of specimens has historically been demonstrated in a number of ways; by physically removing the outer layer and comparing infrared spectra of the interior [27], by using variable angle ATR-FTIR [37], and by infrared microspectroscopy of cross-sections [20]. The formation of a discrete oxidised layer is commonly considered to be a consequence of diffusion-limited oxidation (DLO) mechanisms, whereby

the penetration of oxygen into the network dictates reaction kinetics [54]. This is problematic for accelerated aging studies carried out at elevated temperatures, since the extent of chemical and physical gradients towards the polymer-air interface, and lack of degradation in the bulk, can lead to erroneous lifetime prediction models [55]. Whilst the present study is focused on the chemistry of auto-oxidation rather than kinetics or lifetime prediction, consideration of DLO is important, since there is also some evidence that for epoxy amines, photolysis in the absence of oxygen yields different reaction products from those produced by photo-oxidative degradation [10,13]. Hence, in this study it is possible that any contribution of thermolysis in oxygen depleted regions may similarly differ and skew the interpretation of FTIR spectra. Note that since the FTIR results presented above rely on ATR sampling, the sampling depth is limited to several microns in the case of a diamond IRE (Fig. 1) and <500 nm in the case of the more sensitive Germanium IRE (Fig. 2). According to the literature, for epoxy-amine films of 10  $\mu\text{m}$ –20  $\mu\text{m}$  thickness diffusion limited oxidation (DLO) kinetics are not considered relevant, and oxidation proceeds homogeneously [54,55]. On the other hand, cross-sectional micro-FTIR investigations have also clearly shown that chemical gradients are established at that length scale [55].

In order to investigate whether chemical gradients at the surface of oxidised resins correspond to different local mechanisms (evidenced by e.g., a variation in the oxidation product ratios or position of absorption bands), we adopted the newly developed AFM-IR technique. For AFM-IR analysis, thin films (100  $\mu\text{m}$ ) of resin were prepared in contact with a 40 nm sputtered iron layer supported on cellulose acetate. These were aged for 4 weeks at 70 °C and 14% RH, and then used to prepare ultrathin sections (200 nm thickness) for cross-sectional AFM-IR analysis. We previously demonstrated that this approach is sufficiently sensitive to map the native nanostructural heterogeneity in epoxy-phenolic resins [56–58] and to rule out the spontaneous formation of microscale chemical gradients in DGEBA-TETA epoxy-amine coatings applied to iron substrates [59].

The acquisition of local AFM-IR spectra was achieved by holding the AFM probe in contact with the cross-section surface, and stepping the pulsed infrared laser incident through the fingerprint region wavelengths. The recorded signal corresponded to the amplitude of the probe vibration induced by the thermal expansion of the specimen in response to the pulsed radiation. This process

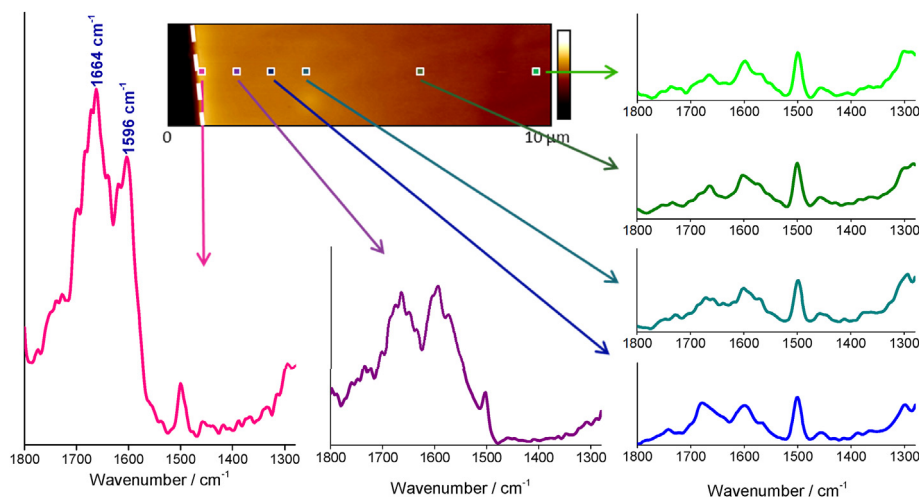


**Fig. 6.** AFM-IR spectra obtained at the outer edge of a 200 nm thick cross-section of an epoxy-amine resin aged for 4 weeks at 70 °C at 14% RH. Spectra were obtained at the locations indicated by markers on the 10  $\mu\text{m}$   $\times$  3  $\mu\text{m}$  contact mode height image shown, and are scaled to the aromatic 1504  $\text{cm}^{-1}$  band. The z scale bar of the AFM image corresponds to 500 nm.

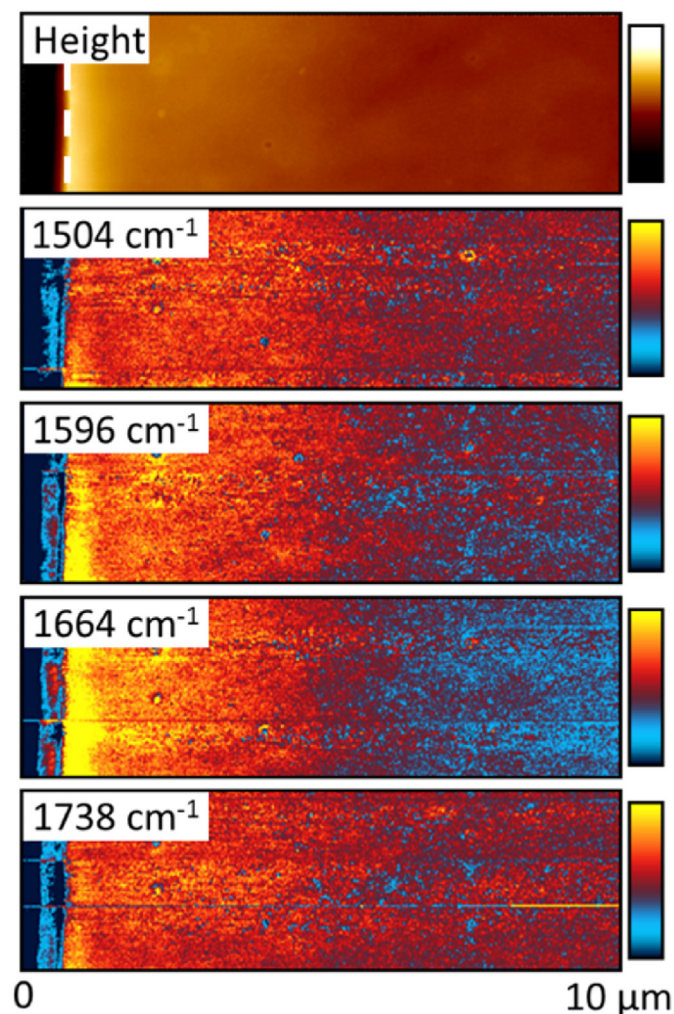


**Fig. 7.**  $10\ \mu\text{m} \times 3\ \mu\text{m}$  resonance enhanced contact mode AFM-IR images of the outer region of a 200 nm thick cross-section of an epoxy-amine resin aged for 4 weeks at  $70\ ^\circ\text{C}$  at 14% RH. The outer edge of the cross-section (corresponding to the polymer-air interface) is located on the left, and is indicated by a dashed white line in the height image. Z scale bar corresponds to 500 nm for the height image, and 0.15 V for the infrared maps.

was repeated at locations with  $1\ \mu\text{m}$  spacing across the outer  $10\ \mu\text{m}$  of the cross-section, Fig. 6.

Towards the outer surface of specimens (marked by a dashed white line in Fig. 6), two broad oxidation bands, with maxima at  $1596\ \text{cm}^{-1}$  and  $1664\ \text{cm}^{-1}$ , were found to dominate the local AFM-IR spectra. The position of these broad bands corresponds well with those found for the difference FTIR spectrum, Fig. 3b. Unlike in the FTIR spectra however, where the spectral differences were slight, AFM-IR of the oxidised interphase allows us to unambiguously identify that both bands are present in resin spectra. Whilst some spontaneous oxidation of the resin sections cannot be ruled out, the contribution of these oxidation bands, relative to the aromatic peak at  $1504\ \text{cm}^{-1}$ , falls off dramatically for AFM-IR spectra obtained further towards the interior of the resin. Thus, in keeping with previous reports, it can be concluded that the oxidation products responsible for the changes in ATR-FTIR spectra after accelerated aging (with a sampling depth of  $<500\ \text{nm}$  due to the Ge IRE used) are heavily concentrated towards the surface of resins. This conclusion was further supported by AFM-IR infrared maps, Fig. 7. The presence of both bands associated with azadiene formation throughout the sampled region also definitively rules out the

alternative explanation of oxidation of a surface layer of unreacted amine. Furthermore, in keeping with FTIR results, no evidence of carbonyl formation was found during the early stages of oxidation.

#### 4. Conclusions

A combination of FTIR microspectroscopy, in-situ heat-controlled FTIR spectroscopy, Raman spectroscopy and the recently developed AFM-IR technique were applied to investigate the auto oxidation of epoxy-amine resins under mild conditions ( $70\ ^\circ\text{C}$ ), producing chemical changes representative of those induced by prolonged natural weathering. As expected, epoxy-amine resin oxidation is characterised by the growth of two infrared absorption bands: the first, appearing at  $1658\ \text{cm}^{-1}$ , is associated with amine cross-linker oxidation, the second, at  $1738\ \text{cm}^{-1}$ , is detected only after 38 days induction period, and is symptomatic of the well-known oxidation mechanism of the DGEBA part of the resin. In order to identify the mechanism of amine oxidation, chemical changes accompanying the early stages of oxidation were isolated after just 28 days aging, and analysed using a range of advanced vibrational spectroscopy tools. Furthermore, auto-oxidation of the molecular amine cross-linker was also fully characterised. Significant parallels were found to exist between the aliphatic amine oxidation products and those found in the resins during the early stages of thermal aging, and as a result, we propose that oxidation of amine groups initiates in the same manner: via the formation of aminium radical cations by one electron oxidation of the incorporated amine groups. Furthermore, we find evidence that the well-known amine oxidation band appearing at  $1658\ \text{cm}^{-1}$  corresponds to the formation of azadiene groups stabilised by conjugation.

#### Declaration of competing interest

The authors declare that they have no known competing financial interests or personal relationships that could have appeared to influence the work reported in this paper.

#### CRediT authorship contribution statement

**Suzanne Morsch:** Conceptualization, Methodology, Investigation, Writing - original draft. **Yanwen Liu:** Investigation. **S.B. Lyon:** Writing - review & editing, Supervision. **S.R. Gibbon:** Writing - review & editing, Supervision. **Benjamin Gabriele:** Investigation. **Mikhail Malanin:** Methodology, Investigation, Writing - review & editing. **Klaus-Jochen Eichhorn:** Conceptualization, Methodology, Writing - review & editing, Supervision.

#### Acknowledgments

S. Morsch is grateful to the Leibniz-Institut für Polymerforschung Dresden e.V., for financial support, S. Morsch and Y. Liu also acknowledge AkzoNobel, and the EPSRC (grant number EP/S004963/1) for materials and financial support. Benjamin Gabriele thanks Roche and the University of Manchester for funding.

#### References

- [1] S.B. Lyon, R. Bingham, D.J. Mills, *Advances in corrosion protection by organic coatings: what we know and what we would like to know*, Prog. Org. Coating 102 (2017) 2–7.
- [2] G.M. Odegard, A. Bandyopadhyay, *Physical aging of epoxy polymers and their composites*, J. Polym. Sci., Part B: Polym. Phys. 49 (2011) 1695–1716.
- [3] G.Z. Xiao, M.E.R. Shanahan, *Irreversible effects of hygrothermal aging on DGEBA/DDA epoxy resin*, J. Appl. Polym. Sci. 69 (1998) 363–369.
- [4] S.G. Prolongo, G. Del Rosario, A. Ureña, *Comparative study on the adhesive properties of different epoxy resins*, Int. J. Adhesion Adhes. 26 (2006)

- 125–132.
- [5] Y.C. Lin, X. Chen, H.J. Zhang, Z.P. Wang, Effects of hygrothermal aging on epoxy-based anisotropic conductive film, *Mater. Lett.* 60 (2006) 2958–2963.
- [6] A.E. Krauklis, A.T. Echtermeyer, Mechanism of yellowing: carbonyl formation during hygrothermal aging in a common amine epoxy, *Polymers* 10 (2018) 1017.
- [7] L. Belec, T.H. Nguyen, D.L. Nguyen, J.F. Chailan, Comparative effects of humid tropical weathering and artificial ageing on a model composite properties from nano- to macro-scale, *Composites, Part A* 68 (2015) 235–241.
- [8] V. Bellenger, J. Verdu, Photooxidation of amine crosslinked epoxies II. Influence of structure, *J. Appl. Polym. Sci.* 28 (1983) 2677–2688.
- [9] A. Rivaton, L. Moreau, J.L. Gardette, Photo-oxidation of phenoxy resins at long and short wavelengths - I. Identification of the photoproducts, *Polym. Degrad. Stabil.* 58 (1997) 321–332.
- [10] B. Mailhot, S. Morlat-Thérias, P.O. Bussière, J.L. Gardette, Study of the degradation of an epoxy/amine resin, 2 kinetics and depth-profiles, *Macromol. Chem. Phys.* 206 (2005) 585–591.
- [11] V. Ollier-Dureault, B. Gosse, Photooxidation of anhydride-cured epoxies: FTIR study of the modifications of the chemical structure, *J. Appl. Polym. Sci.* 70 (1998) 1221–1237.
- [12] A. Rivaton, L. Moreau, J.L. Gardette, Photo-oxidation of phenoxy resins at long and short wavelengths - II. Mechanisms of Formation of photoproducts, *Polym. Degrad. Stabil.* 58 (1997) 333–339.
- [13] B. Mailhot, S. Morlat-Thérias, M. Ouahioune, J.L. Gardette, Study of the degradation of an epoxy/amine resin, 1 photo- and thermo-chemical mechanisms, *Macromol. Chem. Phys.* 206 (2005) 575–584.
- [14] L. Monney, R. Belali, J. Vebrel, C. Dubois, A. Chabaudet, Photochemical degradation study of an epoxy material by IR-ATR analysis, *Polym. Degrad. Stabil.* 62 (1998) 353–359.
- [15] C. Dubois, L. Monney, N. Bonnet, A. Chabaudet, Degradation of an epoxy-glass-fibre laminate under photo-oxidation/leaching complementary constraints, *Composites, Part A* 30 (1999) 361–368.
- [16] A. Meiser, W. Possart, Epoxy-metal interphases: chemical and mechanical aging, *J. Adhes.* 87 (2011) 313–330.
- [17] F. Delor-Jestin, D. Drouin, P.Y. Cheval, J. Lacoste, Thermal and photochemical ageing of epoxy resin - influence of curing agents, *Polym. Degrad. Stabil.* 91 (2006) 1247–1255.
- [18] C. Damian, E. Espuche, M. Escoubes, Influence of three aging types (thermal oxidation, radiochemical and hydrolytic aging) on the structure and gas transport properties of epoxy-amine resins, *Polym. Degrad. Stabil.* 72 (2001) 447–458.
- [19] C. Bockenheimer, D. Fata, W. Possart, New aspects of aging in epoxy networks. I. Thermal aging, *J. Appl. Polym. Sci.* 91 (2004) 361–368.
- [20] A. Meiser, K. Willstrand, W. Possart, Influence of composition, humidity, and temperature on chemical aging in epoxies: a local study of the interphase with air, *J. Adhes.* 86 (2010) 222–243.
- [21] P. Jajibabu, G.D.J. Ram, A.P. Deshpande, S.R. Bakshi, Effect of carbon nano-filler addition on the degradation of epoxy adhesive joints subjected to hygrothermal aging, *Polym. Degrad. Stabil.* 140 (2017) 84–94.
- [22] T. Nguyen, X. Gu, M. Vanlandingham, E. Byrd, R. Rytz, J.W. Martin, Degradation modes of crosslinked coatings exposed to photolytic environment, *J. Coating Technol. Res.* 10 (2013) 1–14.
- [23] B. Mailhot, S. Morlat-Thérias, P.O. Bussière, L. Le Pluaret, J. Duchet, H. Sautereau, J.F. Gérard, J.L. Gardette, Photoageing behaviour of epoxy nanocomposites: comparison between spherical and lamellar nanofillers, *Polym. Degrad. Stabil.* 93 (2008) 1786–1792.
- [24] X. Gu, T. Nguyen, M. Oudina, D. Martin, B. Kidah, J. Jasmin, A. Rezig, L. Sung, E. Byrd, J.W. Martin, D.L. Ho, Y.C. Jean, Microstructure and morphology of amine-cured epoxy coatings before and after outdoor exposures - an AFM study, *J. Coating Technol. Res.* 2 (2005) 547–556.
- [25] A. Rezig, T. Nguyen, D. Martin, L. Sung, Relationship between chemical degradation and thickness loss of an amine-cured epoxy coating exposed to different UV environments, *J. Coating Technol. Res.* 3 (2006) 173–184.
- [26] K. Li, K. Wang, M.S. Zhan, W. Xu, The change of thermal-mechanical properties and chemical structure of ambient cured DGEBA/TEPA under accelerated thermo-oxidative aging, *Polym. Degrad. Stabil.* 98 (2013) 2340–2346.
- [27] S.G. Miller, G.D. Roberts, J.L. Bail, L.W. Kohlman, W.K. Binienda, Effects of hygrothermal cycling on the chemical, thermal, and mechanical properties of 862/W epoxy resin, *High Perform. Polym.* 24 (2012) 470–477.
- [28] C. Galant, B. Fayolle, M. Kuntz, J. Verdu, Thermal and radio-oxidation of epoxy coatings, *Prog. Org. Coating* 69 (2010) 322–329.
- [29] D. Lin-Vien, N.B. Colthup, W.G. Fateley, J.G. Grasselli, *The Handbook of Infrared and Raman Characteristic Frequencies of Organic Molecules*, Academic Press Ltd, London, 1991.
- [30] G. Socrates, *Infrared and Raman Characteristic Group Frequencies: Tables and Charts*, John Wiley & Sons, Ltd., 2004.
- [31] A. Dazzi, C.B. Prater, AFM-IR: technology and applications in nanoscale infrared spectroscopy and chemical imaging, *Chem. Rev.* 117 (2017) 5146–5173.
- [32] B. Lahiri, G. Holland, A. Centrone, Chemical imaging beyond the diffraction limit: experimental validation of the PTIR technique, *Small* 9 (2013) 439–445.
- [33] S. Morsch, S. Lyon, S.R. Gibbon, The degradation mechanism of an epoxy-phenolic can coating, *Prog. Org. Coating* 102 (2017) 37–43.
- [34] D. Khanal, A. Kondyurin, H. Hau, J.C. Knowles, O. Levinson, I. Ramzan, D. Fu, C. Marcott, W. Chrzanosowski, Biospectroscopy of nanodiamond-induced alterations in conformation of intra- and extracellular proteins: a nanoscale IR study, *Anal. Chem.* 88 (2016) 7530–7538.
- [35] C. Bartlam, S. Morsch, K.W.J. Heard, P. Quayle, S.G. Yeates, A. Vijayaraghavan, Nanoscale infrared identification and mapping of chemical functional groups on graphene, *Carbon* 139 (2018) 317–324.
- [36] F. Tang, P. Bao, Z. Su, Analysis of nanodomain composition in high-impact polypropylene by atomic force microscopy-infrared, *Anal. Chem.* 88 (2016) 4926–4930.
- [37] G.A. Luoma, R.D. Rowland, Environmental degradation of an epoxy resin matrix, *J. Appl. Polym. Sci.* 32 (1986) 5777–5790.
- [38] B. Dao, J. Hodgkin, J. Krstina, J. Mardel, W. Tian, Accelerated aging versus realistic aging in aerospace composite materials. I. The chemistry of thermal aging in a low-temperature-cure epoxy composite, *J. Appl. Polym. Sci.* 102 (2006) 4291–4303.
- [39] D.F. Coker, J.R. Reimers, R.O. Watts, The infrared absorption spectrum of water, *Aust. J. Phys.* 35 (1982) 623–638.
- [40] K. Robinson, A. McCluskey, M.I. Attalla, An FTIR spectroscopic study on the effect of molecular structural variations on the CO<sub>2</sub> absorption characteristics of heterocyclic amines, *ChemPhysChem* 12 (2011) 1088–1099.
- [41] K. Robinson, A. McCluskey, M.I. Attalla, An ATR-FTIR study on the effect of molecular structural variations on the CO<sub>2</sub> absorption characteristics of heterocyclic amines, part II, *ChemPhysChem* 13 (2012) 2331–2341.
- [42] D.L. Thompson, K.B. Wagoner, U. Schulze, B. Voit, D. Jehnichen, M. Malanin, Spectroscopic examinations of hydrogen bonding in hydroxy-functionalized ADMET chemistry, *Macromol. Rapid Commun.* 36 (2015) 60–64.
- [43] K.N.T. Tseng, A.M. Rizzi, N.K. Szymczak, Oxidant-free conversion of primary amines to nitriles, *J. Am. Chem. Soc.* 135 (2013) 16352–16355.
- [44] K.M. Lambert, J.M. Bobbitt, S.A. Eldirany, K.B. Wiberg, W.F. Bailey, Facile oxidation of primary amines to nitriles using an oxoammonium salt, *Org. Lett.* 16 (2014) 6484–6487.
- [45] D.H. Rosenblatt, G.T. Davis, L.A. Hull, G.D. Fobberg, Oxidations of amines. V. Duality of mechanism in the reactions of aliphatic amines with permanganate, *J. Org. Chem.* 33 (1968) 1649–1650.
- [46] J.R.L. Smith, L.A.V. Mead, Amine oxidation. Part VII. The effect of structure on the reactivity of alkyl tertiary amines towards alkaline potassium hexacyanoferrate(III), *J. Chem. Soc., Perkin Trans. 2* (1973) 206–210.
- [47] C.A. Audeh, J.R.L. Smith, Amine oxidation. Part II. The oxidation of some trialkylamines with alkaline potassium hexacyanoferrate (III), *J. Chem. Soc. B* (1970) 1280–1285.
- [48] A.L.J. Beckwith, P.H. Eichinger, B.A. Mooney, R.H. Prager, Amine autoxidation in aqueous solution, *Aust. J. Chem.* 36 (1983) 719–739.
- [49] M.J. Chen, J.C. Linehan, J.W. Rathke, Autoxidation of trimethylamine in aqueous solutions, *J. Org. Chem.* 55 (1990) 3233–3236.
- [50] J. Hu, J. Wang, T.H. Nguyen, N. Zheng, The chemistry of amine radical cations produced by visible light photoredox catalysis, *Beilstein J. Org. Chem.* 9 (2013) 1977–2001.
- [51] S. Chi, G.T. Rochelle, Oxidative degradation of monoethanolamine, *Ind. Eng. Chem. Res.* 41 (2002) 4178–4186.
- [52] Y. Amatatsu, Y. Hamada, M. Tsuboi, FTIR detection of unstable molecules: infrared spectrum of 2-azabutadiene, *J. Mol. Spectrosc.* 123 (1987) 276–285.
- [53] G. Keresztury, S. Holly, M.P. Marzocchi, Vibrational spectra of crystalline dimethylglyoxime, HONCCH<sub>3</sub>CH<sub>3</sub>CNOH, *Spectrochim. Acta, Part A* 33 (1977) 29–36.
- [54] M.C. Celina, A.R. Dayile, A. Quintana, A perspective on the inherent oxidation sensitivity of epoxy materials, *Polymer* 54 (2013) 3290–3296.
- [55] E. Ernault, J. Dirrenberger, E. Richaud, B. Fayolle, Prediction of stress induced by heterogeneous oxidation : case of epoxy/amine networks, *Polym. Degrad. Stabil.* 162 (2019) 112–121.
- [56] S. Morsch, Z. Kefallinou, Y. Liu, S.B. Lyon, S.R. Gibbon, Controlling the nanostructure of epoxy resins: reaction selectivity and stoichiometry, *Polymer* 143 (2018) 10–18.
- [57] S. Morsch, Y. Liu, P. Greensmith, S.B. Lyon, S.R. Gibbon, Molecularly controlled epoxy network nanostructures, *Polymer* 108 (2017) 146–153.
- [58] S. Morsch, Y. Liu, S.B. Lyon, S.R. Gibbon, Insights into epoxy network nanostructural heterogeneity using AFM-IR, *ACS Appl. Mater. Interfaces* 8 (2016) 959–966.
- [59] S. Morsch, Y. Liu, M. Malanin, P. Formanek, K.-J. Eichhorn, Exploring whether a buried nanoscale interphase exists within epoxy-amine coatings: implications for adhesion, fracture toughness, and corrosion resistance, *ACS Appl. Nano Mater.* 2 (2019) 2494–2502.